Tubular J-aggregates of cyanine dyes in the near infrared

Austin D. Bailey[a], Arundhati P. Deshmukh[a], Timothy L. Atallah[c], Monica Pengshung[a], Ulugbek Barotov[b], Ellen M. Sletten[a], and Justin R. Caram*[a]

[a]*Department of Chemistry and Biochemistry, University of California, Los Angeles, Los Angeles, California-90095, United States.*

[b]*Department of Chemistry, Massachusetts Institute of Technology, Cambridge, MA 02139*

[c]*Department of Chemistry and Biochemistry, Denison University, Granville, OH, 43023, USA*

Developing improved organic infrared emitters has wide-ranging applicability in fields such as bioimaging or energy harvesting. We synthesize redshifted analogues of C8S3, a well-known cyanine dye that self assembles into tubular aggregates which have attracted widespread attention as artificial photosynthetic complexes. Despite the elongated dye structure, the new pentamethine dyes retain their tubular self-assembly and emit at near-infrared wavelengths. Cryo-electron microscopy and detailed photophysical characterization of the new aggregates reveal similar absorption lineshapes with ~100 nm of redshift, as well as supramolecular morphologies that resemble their trimethine counterparts; the pentamethine aggregates generally show more disorder and decreased superradiance, suggesting that more ordered structures yield more robust photophysical properties. These results provide design principles of superradiant organic emitters, expand the chemical space of near-infrared aggregates, and introduce two additional wavelength-specific antennae as model systems for study.

Molecular aggregates are non-covalently bound self-assemblies of organic chromophores known for their strong absorption and emission properties. The relative arrangement of the dyes deeply affects the excitonic/photophysical properties, e.g. a completely cofacial arrangement of dyes leads to an H-aggregate (less emissive species blueshifted relative to the monomer), whereas a slipped arrangement of chromophores yields J-aggregation (highly emissive species redshifted relative to the monomer).[1,2] J-aggregates are of great importance due to their high oscillator strength, radiative rates, and brightness, making them well-suited for photophysical applications such as penetrative imaging or energy harvesting.[3–6] Additionally, J-aggregates can take on many supramolecular morphologies such as sheets, ribbons, or tubes, leading to different photophysical properties.[7,8]

In particular, tubular J-aggregates show narrow spectral features indicative of only weak disorder—characteristics also identified in nature's most efficient photosynthetic systems.[9–13] Additionally, tubular aggregates have the advantage of a 2D density of states while maintaining directional energy flow.[14,15] This work marks one of the first few examples of a cyanine dye that assembles into tubular J-aggregates (Figure 1A) with emission in the near-infrared (NIR, 700-1000 nm)[16,17], a region where enhanced light penetration enables technological applications.[18–20]

To address this challenge, we modified the structure of an extant chromophore, known as C8S3 (Figure 1B, structure **1a**), that forms superradiant tubular aggregates in the visible region. C8S3 was first introduced to the literature in 1997[21] and has since been studied extensively as a model system for as exciton transport, antenna effects, superradiance and quantum coherence.[14,22–29] Recent work used synthetic modifications on the C8S3 monomer to affect aggregation properties; larger halogen substitutions have been shown to increase the tube diameter, while placement of the halogen atoms was found to be critical in achieving H- vs. J-aggregation.[30,31] Here, we expand this body of work by synthesizing elongated C8S3 dyes with redshifted absorption and emission.

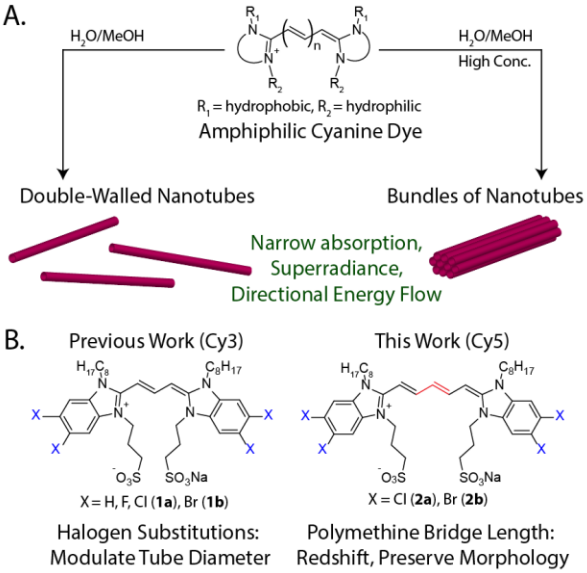

Figure 1. A. Self-assembly of amphiphilic cyanine dyes into J-aggregate nanostructures. **B.** Synthetic modifications on C8S3 (**1a**) in prior work (modifying halogen substitution/placement) and this work (trimethine to pentamethine).

The traditional method to bathochromically shift cyanine dyes is to increase the polymethine chain by one vinylene unit, thereby inducing a ~3,000 cm^{-1} redshift.[32] We use this method to synthesize pentamethine dyes **2a** and **2b** (as opposed to trimethines **1a** and **1b** in the past) based on the C8S3 heterocycle, allowing us to access tubular aggregates of cyanine dyes with NIR emission. Additionally, we explore how that modification (i.e. trimethine to pentamethine) affects the self-assembly and photophysical properties of the aggregates.

The C8S3 heterocycles (**S5**, **S10**) and **1a**/**1b** were synthesized via a literature precedent.[30] The pentamethine cyanines **2a** and **2b** were synthesized by heating the aforementioned heterocycle (**S5**, **S10**) and electrophilic linker (malonaldehyde bisphenylimine HCl) in the presence of a sterically hindered base (1,8-diazabicycloundecene, DBU) in dimethylformamide (Scheme S1). A heptamethine analog of the chlorine derivative was briefly investigated, but ultimately not pursued due to rapid degradation in methanol, which prevented aggregation and further characterization (Scheme S10, Figure S1).

Aggregates of each chromophore were prepared by first creating a stock solution of the dye in methanol. To a small volume of this stock solution was added ultrapure H_2O. The final concentration and methanol/water ratio in each solution were varied. A complete procedure for preparing aggregates is included in SI Section 4. UV-Vis absorption was used to characterize the aggregates, which display a different spectral signature for each morphology.

In methanol, the pentamethine dye monomers absorb at λ_{max} = 616 nm (**2a**) and 614 nm (**2b**) as opposed to the trimethine dyes with λ_{max} = 522 nm (**1a**) and 523 nm (**1b**). Prior work on molecules **1a** and **1b** has shown that the two primary aggregate absorption features occur from the assembly of long double-walled nanotubes (DWNT) and the subsequent bundling of those nanotubes (Figure 2A). The DWNT produces several absorption peaks, namely at 599 and 589 nm, corresponding to the inner and outer walls of the tube respectively.[25] Additionally, both the inner and outer wall show features which have been assigned to parallel (599 nm) and perpendicular (580 nm) excitonic transitions, which are indicative of macroscopic exciton delocalization around each tubular structure.[33] The bundled nanotubes retain a prominent 603 nm feature but also have a less intense, broad absorption around 580 nm.

To probe the aggregate morphologies of the new pentamethine dyes, we both screened **2a** and **2b** at a constant concentration and varied the methanol/water ratio, as well as varied the concentration at a constant methanol/water ratio.[34] Absorbance spectra for monomers and aggregates of different compounds are shown in Figure 2A. In this exploration, we found that the pentamethine dye aggregates display similar photophysical properties to the trimethine dyes, forming two primary aggregates (confirmed by non-negative matrix factorization, Figure S3) depending on the concentration and methanol ratio. One aggregate shows distinct features at 740 and 731 nm (achieved at low concentration, 0.01 mM, 10% methanol), while the other has broad absorption around 715 nm and retains the 745 nm feature (achieved at higher than 0.1 mM, 10% methanol).

Upon identifying appropriate conditions for each aggregate with unique spectral signatures, we performed cryo-EM to determine their supramolecular morphologies. Cryo-EM for the bundled aggregate morphologies of **2a**/**2b** and DWNT morphologies of **1a**/**1b** is shown in Figure 1B; details on cryo-EM technique are in SI Section 6. We originally hypothesized that, like **1a**, **2a** and **2b** would form DWNTs and bundles of nanotubes. The imaging experiments for the high concentration aggregate clearly showed bundles analogous to **1a**; however, the aggregates prepared at 0.01 mM (with features at 746 and 731 nm) did not have sufficient sample density to determine morphology via EM. Additionally, at higher concentrations, these aggregates were found via UV-vis to rapidly convert to the bundled morphology (see SI Section 5). We hypothesize that this short-lived kinetic intermediate (KI, green, Figure 2A) represents DWNTs, though we were unable to confirm this based on electron microscopy.

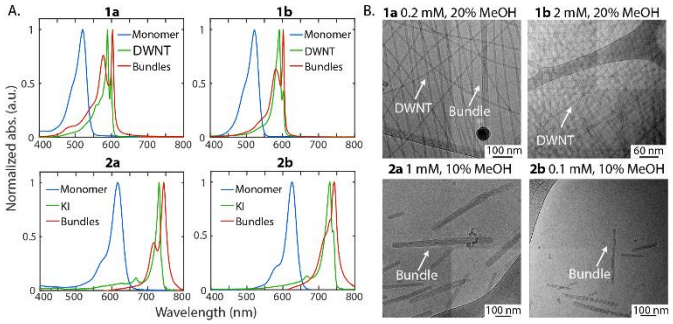

Figure 2. Morphological characterization of monomers and aggregates of **1a**, **1b**, **2a**, and **2b**. **A.** Absorption spectrum of trimethine (**1a** and **1b**) and pentamethine (**2a** and **2b**) dye monomers (100% MeOH) and aggregates (DWNT = double-walled nanotube, KI = kinetic intermediate) **B**. Cryo-electron microscopy images of trimethine (**1a** and **1b**) double-walled nanotubes and pentamethine (**2a** and **2b**) bundles.

Thus, increasing the length of the polymethine bridge has a strong effect on the supramolecular packing of these chromophores. Trimethines **1a** and **1b** clearly have a propensity to form individual DWNTs, while pentamethines **2a** and **2b** almost exclusively form bundles. We hypothesize that the pentamethine dyes aggregate more readily due to the increase in size (more pi-pi stacking area) and hydrophobicity, as well as increased polarizability. Additionally, the bundles are likely the thermodynamic minimum of these aggregates, and therefore stronger non-covalent interactions in the assembly may mean a lower kinetic barrier to bundle formation. Overall, we observed few differences in the aggregates formed from **2a** and **2b**, with the exception of broader linewidths for the brominated dyes, possibly indicating a higher level of disorder in those nanostructures.

Following the identification of the various aggregate morphologies, we probed the photophysical properties of **2a** and **2b** in comparison to **1a** and **1b** (Table 1). We used quantum yields (QY, Φ_F), energy gaps (E_g), and fluorescence lifetimes (τ) to obtain the transition dipole moment (TDM, μ) for each compound's electronic transitions, as well as each aggregate morphology's excitonic transitions. Transition dipole moments are a direct measure of how strongly these materials interact with light, making this value a critical component of this analysis. The emission spectra of **2a** are given in Figure 3A, as well as the lifetimes and fittings in Figure 3B. A full explanation of the photophysical characterization and derivation of TDM can be found in SI Sections 7-9. Photophysical data used in the calculation of TDM are given in Table 1.

Table 1. Photophysical data for monomers and aggregates of dyes **1a**, **1b**, **2a**, and **2b**. [a]Values taken from literature.[30,35] Quantum yield (Φ_F) error was taken as the standard deviation of triplicate measurements. Lifetime (τ) error was taken from the 95% confidence interval in fitting. Error in radiative rate (k_r) and superradiance parameter (η_{SR}) were propagated from the original lifetime and quantum yield measurements.

Compound	Morphology	Φ_F	Avg. τ (ps)	k_r *10^8 (s^{-1})	E_g (nm)	μ (D)	η_{SR}
1a	Monomer	0.025 ± 0.002	202 ± 1	1.2 ± 0.1	528	6.8 ± 0.3	
1a	DWNT	0.15 ± 0.020[a]	140 ± 2	20 ± 2	597	33 ± 2	23.2 ± 0.8
1a	Bundle	0.036 ± 0.004	81 ± 1	7.3 ± 0.7	602	20 ± 1	8.7 ± 0.3
1b	Monomer	0.028 ± 0.002	220 ± 1	1.3 ± 0.1	530	6.9 ± 0.1	
1b	DWNT	0.040 ± 0.004[a]	68 ± 2	8.1 ± 0.7	593	21 ± 1	9.0 ± 0.2
1b	Bundle	0.013 ± 0.001	62 ± 1	3.2 ± 0.3	603	13.4 ± 0.7	3.8 ± 0.1
2a	Monomer	0.33 ± 0.025	1019 ± 3	3.3 ± 0.2	625	14.2 ± 0.5	
2a	Bundle	0.012 ± 0.001	72 ± 2	2.6 ± 0.3	740	16.3 ± 0.9	1.3 ± 0.1
2b	Monomer	0.36 ± 0.020	1126 ± 2	3.2 ± 0.2	623	14.1 ± 0.4	
2b	Bundle	0.060 ± 0.001	70 ± 1	1.6 ± 0.2	725	12.2 ± 0.6	0.8 ± 0.1

The transition dipole moments for all monomers and aggregates are detailed in Figure 3C. Using these TDM values, we calculated the superradiance parameter η_{SR} for each dye, as shown in equation 1.

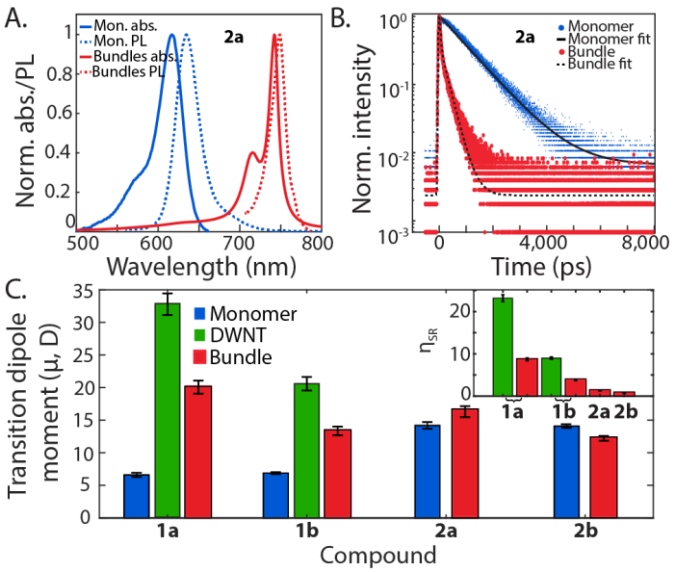

Figure 3. Photophysical characterization of monomers and aggregates of **2a**/**2b**. **A.** Absorption (solid) and photoluminescence (dotted) spectra for **2a** monomer (methanol) and bundle (methanol/water). **B.** Monomer lifetime, bundle lifetime, and corresponding fits for **2a**. **C.** Transition dipole moments for all monomers (blue) and aggregate morphologies (green, red). (Inset: superradiance parameter η_{SR} for each aggregate morphology.)

Although previous works have used different definitions for superradiance in J-aggregate systems[14,36,37], we maintain that this method offers the advantage of factoring in the difference in energy gap, which results in an intrinsic change in radiative rates due to the redshift from monomer to aggregate.[38] The η_{SR} parameter is also a measure of the coherence length for the fluorescent state, or the number of monomers over which the Frenkel excitons delocalize.[39] This value is rigorously defined only for linear aggregates, though it is a useful metric for all aggregate morphologies.

Figure 3C demonstrates that the trimethine aggregates possess transition dipole moments up to 5 times larger than their monomer counterparts; this corresponds to high superradiance parameters (~23 for **1a** DWNT). However, for the pentamethine dyes, the aggregate transition dipoles are comparable to those of the monomers. This accordingly leads to η_{SR} values that are closer to 1, meaning that they are less superradiant (or in the case of **2b**, subradiant). These data can be attributed to the higher disorder in aggregates of **2a** and **2b** which leads to decreased exciton delocalization despite retaining redshifted emission. We also observe that the brominated aggregates are less superradiant than their chlorinated counterparts; we hypothesize this is due to the additional energetic disorder, which is indicated by the broader absorption linewidths and also via structural disorder in the trimethine aggregate cryo-EM.

There is a clear correlation between the heterogeneity of self-assembly and the photophysical properties in these aggregates. For example, the bundles of the trimethine dyes deliver a lower η_{SR} in terms of superradiance than the DWNTs. Similarly, the pentamethine bundles have a lower η_{SR} relative to the trimethine variant, and the **1b**/**2b** (brominated) bundles lower yet than **1a**/**2a** (chlorinated). In general, this suggests that more ordered structures yield higher superradiance. Extrapolating from this connection, the future development of molecular aggregates for photophysical applications should center around achieving uniform supramolecular structures with robust assembly. These results bolster

the need for exploration in structure/property relationships between dye structures and their self-assembly, a topic that remains a fundamental challenge for this field.

In summary, we synthesized and aggregated two new pentamethine dyes based on the C8S3 scaffold to create two new emitters at ~750 nm. We maintain the lineshapes of the original aggregates while redshifting by 100 nm and found with cryo-EM imaging that the pentamethine dyes mainly self-assembled into large bundles of nanotubes, as opposed to long single tubes. Photophysical characterization of these aggregates then allowed us to calculate transition dipole moments and superradiance parameters for each compound and aggregate morphology. Correlating the morphological and photophysical data, we were able conclude that the pentamethine dyes displayed different kinetics of self-assembly that resulted in generally more disordered aggregate bundles with lower superradiance relative to their trimethine comparators. Synthesizing these results, this work introduces two new NIR antennae as models for study and suggests that future works should aim for more ordered assemblies to achieve superradiant aggregates in the near-infrared.

Acknowledgements

This work was supported by NSF CHE grant no. 1905242 and a faculty research grant (UCLA Academic Senate), as well as NSF CHE-1048804. The authors acknowledge the use of instruments at the Electron Imaging Center for NanoMachines supported by the NIH (1S10RR23057) and CNSI at UCLA.

References

1 J. L. Bricks, Y. L. Slominskii, I. D. Panas and A. P. Demchenko, *Methods Appl. Fluoresc.*, 2017, **6**, 012001.

2 F. Würthner, T. E. Kaiser and C. R. Saha-Möller, *Angew. Chemie Int. Ed.*, 2011, **50**, 3376–3410.

3 C. Sun, B. Li, M. Zhao, S. Wang, Z. Lei, L. Lu, H. Zhang, L. Feng, C. Dou, D. Yin, H. Xu, Y. Cheng and F. Zhang, *J. Am. Chem. Soc.*, 2019, **141**, 19221–19225.

4 M. Shakiba, K. K. Ng, E. Huynh, H. Chan, D. M. Charron, J. Chen, N. Muhanna, F. S. Foster, B. C. Wilson and G. Zheng, *Nanoscale*, 2016, **8**, 12618–12625.

5 K. Saito*, *J. Phys. Chem. B*, 1999, **103**, 6579–6583.

6 T. Brixner, R. Hildner, J. Köhler, C. Lambert and F. Würthner, *Adv. Energy Mater.*, 2017, **7**, 1700236.

7 *,† Hans von Berlepsch, ‡ and Stefan Kirstein and C. Böttcher†, *J. Phys. Chem. B*, 2004, **108**, 18725–18733.

8 A. P. Deshmukh, D. Koppel, C. Chuang, D. M. Cadena, J. Cao and J. R. Caram, , DOI:10.1021/acs.jpcc.9b05060.

9 G. S. Engel, T. R. Calhoun, E. L. Read, T. K. Ahn, T. Mančal, Y. C. Cheng, R. E. Blankenship and G. R. Fleming, *Nature*, 2007, **446**, 782–786.

10 G. D. Scholes, G. R. Fleming, A. Olaya-Castro and R. Van Grondelle, *Nat. Chem.*, 2011, 3, 763–774.

11 F. S. Freyria, J. M. Cordero, J. R. Caram, S. Doria, A. Dodin, Y. Chen, A. P. Willard and M. G.

Bawendi, *Nano Lett.*, 2017, **17**, 7665–7674.

12 J. R. Caram and G. S. Engel, *Faraday Discuss.*, 2011, **153**, 93–104.

13 C. Wang and E. A. Weiss, *Nano Lett.*, 2017, **17**, 5666–5671.

14 S. Doria, T. S. Sinclair, N. D. Klein, D. I. G. Bennett, C. Chuang, F. S. Freyria, C. P. Steiner, P. Foggi, K. A. Nelson, J. Cao, A. Aspuru-Guzik, S. Lloyd, J. R. Caram and M. G. Bawendi, *ACS Nano*, 2018, **12**, 4556–4564.

15 C. Chuang, C. K. Lee, J. M. Moix, J. Knoester and J. Cao, , DOI:10.1103/PhysRevLett.116.196803.

16 H. v. Berlepsch and C. Böttcher, *Phys. Chem. Chem. Phys.*, 2018, **20**, 18969–18977.

17 Z. Chen, Y. Liu, W. Wagner, V. Stepanenko, X. Ren, S. Ogi and F. Würthner, *Angew. Chemie Int. Ed.*, 2017, **56**, 5729–5733.

18 S. A. Hilderbrand and R. Weissleder, *Curr. Opin. Chem. Biol.*, 2010, **14**, 71–79.

19 Y. T. Lim, S. Kim, A. Nakayama, N. E. Stott, M. G. Bawendi and J. V. Frangioni, *Mol. Imaging*, 2003, **2**, 50–64.

20 R. Rondão, A. R. Frias, S. F. H. Correia, L. Fu, V. de Z. Bermudez, P. S. André, R. A. S. Ferreira and L. D. Carlos, *ACS Appl. Mater. Interfaces*, 2017, **9**, 12540–12546.

21 A. Pawlik, S. Kirstein, U. De Rossi and S. Daehne, *J. Phys. Chem. B*, 1997, **101**, 5646–5651.

22 D. M. Eisele, C. W. Cone, E. A. Bloemsma, S. M. Vlaming, C. G. F. Van Der Kwaak, R. J. Silbey, M. G. Bawendi, J. Knoester, J. P. Rabe and D. A. Vanden Bout, *Nat. Chem.*, 2012, **4**, 655–662.

23 D. M. Eisele, J. Knoester, S. Kirstein, J. P. Rabe and D. A. Vanden Bout, *Nat. Nanotechnol. 2009 410*, 2009, **4**, 658–663.

24 † Jennifer L. Lyon, ‡ Dörthe M. Eisele, ‡ Stefan Kirstein, ‡ Jürgen P. Rabe, † and David A. Vanden Bout and † Keith J. Stevenson*, *J. Phys. Chem. C*, 2008, **112**, 1260–1268.

25 D. M. Eisele, D. H. Arias, X. Fu, E. A. Bloemsma, C. P. Steiner, R. A. Jensen, P. Rebentrost, H. Eisele, A. Tokmakoff, S. Lloyd, K. A. Nelson, D. Nicastro, J. Knoester and M. G. Bawendi, *Proc. Natl. Acad. Sci. U. S. A.*, 2014, **111**, E3367–E3375.

26 K. Ng, M. Webster, W. P. Carbery, N. Visaveliya, P. Gaikwad, S. J. Jang, I. Kretzschmar and D. M. Eisele, *Nat. Chem. 2020 1212*, 2020, **12**, 1157–1164.

27 J. R. Caram, S. Doria, D. M. Eisele, F. S. Freyria, T. S. Sinclair, P. Rebentrost, S. Lloyd and M. G. Bawendi, *Nano Lett.*, 2016, **16**, 6808–6815.

28 J. Yuen-Zhou, D. H. Arias, D. M. Eisele, C. P. Steiner, J. J. Krich, M. G. Bawendi, K. A. Nelson and A. Aspuru-Guzik, *ACS Nano*, 2014, **8**, 5527–5534.

29 B. Kriete, J. Lüttig, T. Kunsel, P. Malý, T. L. C. Jansen, J. Knoester, T. Brixner and M. S. Pshenichnikov, , DOI:10.1038/s41467-019-12345-9.

30 B. Rn Kriete, A. S. Bondarenko, V. R. Jumde, L. E. Franken, A. J. Minnaard, T. L. C. Jansen, J. Knoester and M. S. Pshenichnikov, *J. Phys. Chem. Lett*, , DOI:10.1021/acs.jpclett.7b00967.

31 S. M. Roth, D. J. Press, B. Heyne and T. C. Sutherland, *J. Org. Chem.*, 2021, **86**, 8651.

32 J. L. Bricks, A. D. Kachkovskii, Y. L. Slominskii, A. O. Gerasov and S. V. Popov, *Dye. Pigment.*, 2015.

33 K. A. Clark, C. W. Cone and D. A. Vanden Bout, , DOI:10.1021/jp409573h.

34 A. P. Deshmukh, A. D. Bailey, L. S. Forte, X. Shen, N. Geue, E. M. Sletten and J. R. Caram, *J. Phys. Chem. Lett.*, 2020, **11**, 8026–8033.

35 F. S. Freyria, J. M. Cordero, J. R. Caram, S. Doria, A. Dodin, Y. Chen, A. P. Willard and M. G. Bawendi, *Nano Lett.*, 2017, **17**, 7665–7674.

36 D. L. Akins, , DOI:10.1021/jp991627a.

37 H. Zhao, Y. Zhao, Y. Song, M. Zhou, W. Lv, L. Tao, Y. Feng, B. Song, Y. Ma, J. Zhang, J. Xiao, Y. Wang, D.-H. Lien, M. Amani, H. Kim, X. Chen, Z. Wu, Z. Ni, P. Wang, Y. Shi, H. Ma, X. Zhang, J.-B. Xu, A. Troisi, A. Javey and X. Wang, *Nat. Commun. 2019 101*, 2019, **10**, 1–9.

38 H. Friedman, E. Cosco, T. Atallah, S. Jia, E. Sletten and J. Caram, , DOI:10.26434/CHEMRXIV.14374493.V1.

39 T. Tsurumi, T.; Hirayama, H.; Vacha, M.; Taniyama, *Nanoscale physics for materials science*, Taylor & Francis, Abingdon, 2010.